5474 *Chem. Mater.* **2009,** *21,* 5474–5484
DOI:10.1021/cm9022776

CHEMISTRY OF MATERIALS
Article

Essential Role of Calcium Phosphate Heterogeneities in 2D-Hexagonal and 3D-Cubic $SiO_2-CaO-P_2O_5$ Mesoporous Bioactive Glasses

A. García,[†,‡] M. Cicuéndez,[†,‡] I. Izquierdo-Barba,[†,‡] D. Arcos,*[,†,‡] and M. Vallet-Regí*[,†,‡]

[†]*Departamento Química Inorgánica y Bioinorgánica, Facultad de Farmacia, Universidad Complutense de Madrid, Plaza Ramón y Cajal s/n, 28040 Madrid, Spain, and* [‡]*Networking Research Center on Bioengineering, Biomaterials and Nanomedicine* (*CIBER-BBN*), *Madrid, Spain*

Received July 24, 2009. Revised Manuscript Received October 5, 2009

Mesoporous bioactive glasses (MBGs) with a compoisition of $85SiO_2-10CaO-5P_2O_5$ (mol %) have been prepared through the evaporation-induced self-assembly (EISA) method, using P123 as a structure directing agent. For the first time, $SiO_2-CaO-P_2O_5$ MBGs with identical composition and textural properties, but exhibiting different bicontinuous 3D-cubic and 2D-hexagonal structures, have been prepared. These materials allow us to discriminate the role of the structure on the bioactivity, from other parameters. To understand the role of each component on the mesostructure, local environment, and bioactive behavior, mesoporous $100SiO_2$, $95SiO_2-5P_2O_5$, and $90SiO_2-10CaO$ (mol %) materials were also prepared under the same conditions. The results demonstrate that the joint presence of CaO and P_2O_5 results in amorphous calcium phosphate (ACP) clusters sited at the pore wall surface. This heterogeneity highly improves the bioactive behavior of these materials. In addition, the presence of ACP clusters within the silica network leads to different mesoporous structures. The mesoporous order can be tuned through a rigorous control of the solvent evaporation temperature during the mesophase formation, resulting in *p6mm*, *p6mm*/*Ia*$\bar{3}$*d* coexistence, and *Ia*$\bar{3}$*d* phases for 20, 30, and 40 °C, respectively. Preliminary results indicate that, in the case of identical composition and textural properties, the mesoporous structure does not have influence on the apatite formation, although initial ionic exchange is slightly enhanced for 3D cubic bicontinuous structures.

Introduction

Mesoporous bioactive glasses (MBGs) are a new generation of bioactive materials that are intended for use to heal and restore bone tissue in orthopedic and periodontal diseases. MBGs were prepared for the first time by Zhao et al. in 2004,[1] and they can be considered as enhanced derivatives of conventional $SiO_2-CaO-P_2O_5$ sol−gel glasses.[2−5] In fact, MBGs preparation is based on the principles of sol−gel processes and supramolecular chemistry of surfactants acting as structure directing agents.[6,7] The results are a new family of compounds with outstanding *in vitro* bioactive behavior. This fact is due to the chemical composition, which is similar to sol−gel bioactive glasses classically prepared,[8−12] together with surfaces and porosities 3−5 times higher than those of conventional sol−gel glasses. In addition, the mesopore ordering provides a final product suitable to be used as a delivery system of drugs and osteogenic agents.[13−15]

During the last five years, MBGs have attracted the attention of many researchers. In this sense, not only powdered MBGs,[16,17] but also microspheres,[18,19] cements,[20]

*Author to whom correspondence should be addressed. E-mails: vallet@farm.ucm.es (M.V.-R.), arcosd@farm.ucm.es (D.A.).

(1) Yan, X. X.; Yu, C. Z.; Zhou, X. F.; Tang, J. W.; Zhao, D. Y. *Angew. Chem., Int. Ed.* **2004**, *43*, 5980–5984.
(2) Li, R.; Clark, A. E.; Hench, L. L. *J. Appl. Biomater.* **1991**, *2*, 231–239.
(3) Peltola, T.; Jokinen, M.; Rahiala, H.; Levänen, E.; Rosenholm, J. B.; Kangasniemi, I.; Yli-Urpo, A. *J. Biomed. Mater. Res.* **1999**, *44*, 12–21.
(4) Vallet-Regí, M.; Ragel, C. V.; Salinas, A. J. *Eur. J. Inorg. Chem.* **2003**, 1029–1042.
(5) Vallet-Regí, M. *Dalton Trans.* **2006**, *44*, 5211–5220.
(6) Hench, L. L.; West, J. K. *Chem. Rev.* **1990**, *90*, 33–72.
(7) Mann, S.; Burkett, S. L.; Davis, S. A.; Fowler, C. E.; Mendelson, N. H.; Sims, S. D.; Walsh, D.; Whilton, N. T. *Chem. Mater.* **1997**, *9*, 2300–2310.
(8) Pereira, M. M.; Clark, A. E.; Hench, L. L. *J. Biomed. Mater. Res.* **1994**, *28*, 693–698.
(9) Vallet-Regí, M.; Arcos, D.; Pérez-Pariente, J. *J. Biomed. Mater. Res.* **2000**, *51*, 23–28.
(10) Izquierdo-Barba, I; Salinas, A. J.; Vallet-Regí, M. *J. Biomed. Mater. Res.* **1999**, *47*, 243–250.
(11) Jones, J. R.; Hench, L. L. *J. Mater. Sci.* **2003**, *38*, 3783–3790.
(12) Jokinen, M.; Rahiala, H.; Rosenholm, J. B.; Peltola, T.; Kangasniemi, I. *J. Sol-Gel Sci. Technol.* **1998**, *12*, 159–167.
(13) Vallet-Regí, M.; Balas, F.; Arcos, D. *Angew. Chem., Int. Ed.* **2007**, *46*, 7548.
(14) Vallet-Regí, M.; Colilla, M.; Izquierdo-Barba, I. *J. Biomed. Nanotechnol.* **2008**, *4*, 1–15.
(15) Vallet-Regí, M.; Balas, F.; Colilla, M.; Manzano, M. *Prog. Solid State Chem.* **2008**, *36*, 163–191.
(16) Yan, X. X.; Deng, H. X.; Huang, X. H.; Lu, G. Q.; Qiao, S. Z.; Zhao, D. Y.; Yu, C. Z. *J. Non-Cryst. Solids* **2005**, *351*, 3209–3217.
(17) Yan, X. X.; Huang, H. H.; Yu, C. Z.; Deng, H. X.; Wang, Y.; Zhang, A. D.; Qiao, S. Z.; Lu, G. Q.; Zhao, D. Y. *Biomaterials* **2006**, *27*, 3396–3403.
(18) Arcos, D.; López-Noriega, A.; Ruiz-Hernández, E.; Terasaki, O.; Vallet-Regí, M. *Chem. Mater.* **2009**, *21*, 1000–1009.
(19) Li, X.; Zhang, L. X; Dong, X. P.; Liang, J.; Shi, J. L. *Microporous Mesoporous Mater.* **2007**, *102*, 151–158.
(20) Shi, Q. H.; Wang, J. F.; Zhang, J. P.; Fan, J.; Stucky, G. D. *Adv. Mater.* **2006**, *18*, 1038–1042.

Published on Web 10/21/2009

and scaffolds[21,22] have been prepared. In addition, functionalization,[23] drug delivery properties,[24,25] and hemostatic activity[26] have been also considered for potential applications of MBGs.

The preparation of MBGs in the $SiO_2-CaO-P_2O_5$ system requires synthesis strategies that lead to robust mesoporous structures. The presence of a multicomponent inorganic system, including CaO, makes it difficult to obtain ordered structures when conventional methods are used for mesoporus materials syntheses. In this sense, the evaporation-induced self-assembly (EISA) method[27] is the best choice to prepare these types of MBGs. This method is based on the preferential evaporation of the organic solvents used initially to homogenize the solution of precursors and surfactant, thus enriching the concentrations of nonvolatile constituents. The consequence is the formation of more-stable mesoporous structures.

Because of the complexity of multicomponent systems during the mesophase formation, the final mesoporous structure is difficult to predict, as well as the local environment of each component. Besides, the role of the pore ordering on the bioactive behavior of MBGs is still unclear. For instance, Yan et al. have reported on the homogeneous Ca distribution within 2D-hexagonal MBGs, because of the nanometric size of the pore walls,[1,16] thus avoiding aggregates or calcium phosphate clusters formation. Hexagonal MBGs have been also obtained using P123 and F127 triblock copolymers and the mesophase formation has been followed via small-angle X-ray diffraction (SAXRD),[28] indicating that the mesophase formation occurs via a complicated process that involves a Si−O−Ca−P−O complex. Yun et al. have also shown the possibilities of preparing MBGs with cubic $Im\bar{3}m$ cage-type structures when F127 is added as a surfactant,[29,30] whereas P123 addition commonly results in 2D-hexagonal *p6mm* structures. However, in 2006, it was demonstrated that bicontinuous 3D-cubic structures could be also been prepared with P123 in the same system, under very similar conditions.[31] The mesoporous structure could be modified by changing the SiO_2/CaO ratio. By varying this ratio, 3D-cubic to 2D-hexagonal evolution could be observed as the amount of CaO increased. Moreover, it was thereafter demonstrated that the bioactive behavior showed special particularities, depending on the molar composition and mesoporous ordering in $SiO_2-CaO-P_2O_5$ system.[32]

It has been hypothesized that 3D-cubic bicontinuous structures can facilitate the bioactive process, because of the better fluids accessibility through an interconnected porous structure.[30,32] However, the mesoporous arrangement is commonly associated to the chemical composition or textural properties in MBGs. Consequently, the different bioactive behavior between 3D-cubic or 2D-hexagonal structures cannot be discriminated from chemical and textural factors or even with the homogeneity degree of Ca^{2+} cations into the silica network, which is also a controversial subject in this field.[33]

For the first time, we have prepared $SiO_2-CaO-P_2O_5$ MBGs with identical composition and textural properties that exhibit different bicontinuous 3D-cubic and 2D-hexagonal structures. We have chosen the composition $85SiO_2-10CaO-5P_2O_5$ (mol %) because of its excellent bioactive behavior without altering the surrounding fluids.[32] These materials allow us to discriminate the role of the structure from other parameters. This paper also reveals the fundamental role of P_2O_5 over the local environment of Ca^{2+}, demonstrating the importance of the calcium phosphate heterogeneities on the final mesoporous structure and bioactive behavior in these compounds.

Materials and Methods

Synthesis. Highly ordered mesoporous materials were synthesized using a nonionic surfactant Pluronic P123 (BASF) as a structure directing agent and evaporation-induced self-assembly (EISA) method. P123 is an amphiphilic triblock polymer that has the following sequence: $EO_{20}PO_{70}EO_{20}$, where EO is poly(ethylene oxide) and PO is poly(propylene oxide). Tetraethyl orthosilicate (TEOS), triethyl phosphate (TEP), and calcium nitrate tetrahydrate ($Ca(NO_3)_2 \cdot 4H_2O$) were used as SiO_2, P_2O_5, and CaO sources, respectively. Four different compositions, denoted as Si100, Si95P5, Si90Ca10, and Si85Ca10P5, were prepared according to the nominal composition (on a mol % basis) of SiO_2 (Si), P_2O_5 (P), and CaO (Ca), respectively.

In a typical synthesis, 16 g of P123 were dissolved in 240 mL of ethanol with 4 mL of 0.5 M HCl solution at room temperature. Afterward, the appropriate amount of TEOS, TEP, and/or $Ca(NO_3)_2 \cdot 4H_2O$ was added under continuous stirring in 3 h intervals. The different amounts of reactive are shown in Table S1 of the Supporting Information. The resulting colorless sols were stirred at room temperature for 24 h, and then they were transferred into Petri dishes (9 cm in diameter). Six aliquots (*ca.* 50 mL) were obtained for each composition and evaporated at three different temperatures (20, 30, and 40 °C) for ~7 days. With this synthesis scheme,

(21) Yun, H.; Kim, S.; Hyeon, Y. *Chem. Commun.* **2007**, 2139–2141.
(22) Li, X.; Shi, J. L.; Dong, X. P.; Zhang, L. X.; Zeng, H. Y. *J. Biomed. Mater. Res.* **2008**, *84A*, 84–91.
(23) Sun, J.; Li, Y. S.; Li, L.; Zhao, W.; Li, L.; Gao, J. H.; Ruan, M. L.; Shi, J. L. *J. Non-Cryst. Solids* **2008**, *354*, 3799–3805.
(24) Zhao, L. Z.; Yan, X. X.; Zhou, X. F.; Zhou, L.; Wang, H. N.; Tang, J. W.; Yu, C. Z. *Microporous Mesoporous Mater.* **2008**, *109*, 210–215.
(25) Xia, W.; Chang, J. *J. Controlled Release* **2006**, *110*, 522–530.
(26) Ostomel, T. A.; Shi, Q.; Tsung, C. K.; Liang, H.; Stucky, G. D. *Small* **2006**, *2*, 1261–1265.
(27) Brinker, C. J.; Lu, Y. F.; Sellinger, A.; Fan, H. Y. *Adv. Mater.* **1999**, *11*, 579–585.
(28) Zhao, Y. F.; Loo, S. C. J.; Chen, Y. Z.; Boey, F. Y. C.; Ma, J. *J. Biomed. Mater. Res.* **2008**, *85A*, 1032–1042.
(29) Yun, H.; Kim, S.; Hyun, Y. *Solid State Sci.* **2008**, *10*, 1083–1092.
(30) Yun, H.; Kim, S.; Hyeon, Y. *Mater. Lett.* **2007**, *61*, 4569–4572.
(31) López-Noriega, A.; Arcos, D.; Izquierdo-Barba, I.; Sakamoto, Y.; Terasaki, O.; Vallet-Regí, M. *Chem. Mater.* **2006**, *18*, 3137–3144.
(32) Izquierdo-Barba, I.; Arcos, D.; Sakamoto, Y.; Terasaki, O.; López-Noriega, A.; Vallet-Regí, M. *Chem. Mater.* **2008**, *20*, 3191–3198.
(33) Leonova, E.; Izquierdo-Barba, I.; Arcos, D.; López-Noriega, A.; Hedin, N.; Vallet-Regí, M.; Edén, M. *J. Phys. Chem. C* **2008**, *112*, 5552–5562.

we modify the thermal conditions at which mesophase formation occurs, thus changing the final mesoporous structure (see below). Finally, homogeneous membranes were obtained and calcined in air at 700 °C for 6 h to obtain ordered mesoporous powders with different chemical compositions.

Characterization. Powder X-ray diffraction (XRD) patterns were recorded in a Philips Model X'Pert diffractometer that used Cu Kα radiation (wavelength of 1.5406 Å). XRD patterns were collected in the 2θ range of 0.6°−8°, with a step size of 0.02° and a counting time of 0.5 s per step.

Transmission electron microscopy (TEM) was performed with a JEOL Model 3000 FEG electron microscope that had been fitted with a double-tilting goniometer stage (±45°) and with an Oxford LINK EDS analyzer. TEM images were recorded using a charge-coupled device (CCD) camera (MultiScan model 794, Gatan, 1024 × 1024 pixels, 24 μm × 24 μm in size) using low-dose condition. Fourier transform (FT) patterns were conducted using Digital Micrograph (Gatan).

The textural properties of the calcined materials were determined by nitrogen adsorption/desorption analyses at −196 °C on a Micromeritics Model ASAP 2020 instrument (Micromeritics Co, Norcross, GA). To perform the N_2 adsorption measurements, 100−150 mg of materials were previously degassed under vacuum for 24 h at 200 °C. The surface area was determined using the Brunauer−Emmett−Teller (BET) method. The pore size distribution in the range of 0.5−40 nm was determined from the desorption branch of the isotherm by means of the Barrett−Joyner−Halenda (BJH) method.

$^{1}H \rightarrow {}^{29}Si$ and $^{1}H \rightarrow {}^{31}P$ CP (cross-polarization)/MAS (magic-angle-spinning) and single-pulse (SP) solid-state nuclear magnetic resonance (NMR) measurements were performed to evaluate the different silicon and phosphorus environments in the synthesized samples. The NMR spectra were recorded on a Bruker Model Avance 400 spectrometer. Samples were spun at 10 kHz for ^{29}Si and 6 kHz in the case of ^{31}P. Spectrometer frequencies were set to 79.49 and 161.97 MHz for ^{29}Si and ^{31}P, respectively. Chemical shift values were referenced to tetramethylsilane (TMS) and H_3PO_4 for ^{29}Si and ^{31}P, respectively. All spectra were obtained using a proton-enhanced CP method, using a contact time of 1 ms. The time period between successive accumulations was 5 and 4 s for ^{29}Si and ^{31}P, respectively, and the number of scans was 10 000 for all spectra.

***In Vitro* Bioactivity Test.** The assessment of *in vitro* bioactivity was performed in a SBF solution, proposed by Kokubo et al.[34] The simulated body fluid (SBF) solution has a composition and concentration similar to those of the inorganic part of human plasma, prepared by dissolving NaCl, KCl, $NaHCO_3$, $K_2HPO_4 \cdot 3H_2O$, $MgCl_2 \cdot 6H_2O$, $CaCl_2$, and Na_2SO_4 into distilled water and buffering at pH 7.4 with tris(hydroxymethyl)aminomethane $NH_2C(CH_2OH)_3$ and HCl.

The four samples with different chemical compositions were used to investigate the composition−bioactivity correlation. For this purpose, 1 g of powder was immersed in 50 mL of filtered SBF in polyethylene containers under sterile conditions. The containers were treated at 37 °C under continuous orbital stirring in an Ecotron HT incubator. After soaking, the powders were collected from the SBF via filtration and air-dried at room temperature. Bioactive behavior was followed over powdered samples by Fourier transform infrared (FTIR) spectroscopy after different soaking periods to determine the formation of an apatite like-phase, according to the method proposed by Warren, Clark, and Hench[35] for bioactive glasses. FTIR spectra were collected in a Thermo Nicolet Model Nexus system that was equipped with a Goldengate attenuated total reflectance (ATR) device and using the KBr pellet method. XRD patterns were collected before and after soaking in SBF with a Philips Model X'pert diffractometer using the Kα Cu radiation. Finally, the Ca^{2+} content and pH evolution of the SBF were tested as a function of MBGs soaking by means of an Ilyte ion analyzer.

Results. Figure 1 shows low-angle XRD patterns of the calcined pure silica sample, Si100, and calcined samples comprised of $SiO_2-P_2O_5$ (Si95P5) and SiO_2-CaO (Si90Ca10), which have been evaporated at 40 °C. Samples exclusively synthesized with network formers (i.e., Si100 and Si95P5) show an intense diffraction maxima at $2\theta = 1.17°$ and 1.18° for Si100 and Si95P5, respectively. These maxima can be indexed as the 211 reflection of a 3D-cubic phase with space group $Ia\bar{3}d$, based on TEM results. A weak shoulder at $2\theta°$ values of ∼2.22° could be assigned to the 400 reflection of the same phase, considering the TEM results (see below). The unit-cell parameters calculated from the 211 peak positions are 18.5 and 18.3 nm for Si100 and Si95P5, respectively. Identical XRD patterns were obtained for these samples, independent of the evaporation temperature at 20, 30, or 40 °C (see Table 1).

When 10% mol of CaO is incorporated (Si90Ca10), the XRD pattern shows two weak peaks beside the first intense peak, which can be indexed assuming a typical 2D-hexagonal *p6mm* structure. The well-resolved peaks can be indexed as 10, 11, and 20 reflections of a more hydrophilic hexagonal structure with a unit-cell parameter of 8.2 nm (see TEM results below). This composition also showed identical mesopore ordering that was independent of evaporation temperature (see Table 1), noting that the presence or absence of CaO as a network modifier can determine the formation of more hydrophilic (*p6mm*) or hydrophobic ($Ia\bar{3}d$) structures, respectively.

Figure 2 shows the XRD patterns of the calcined Si85Ca10P5 sample, when the EISA process was performed at 20, 30, and 40 °C. In this case, the mesopore structure is

(34) Kokubo, T.; Kushitani, H.; Sakka, S.; Kitsugi, T.; Yamamuro, T. *J. Biomed. Mater. Res.* **1990**, *24*, 721–734.

(35) Warren, L. D.; Clark, A. E.; Hench, L. L. *J. Biomed. Mater. Res.: Appl. Biomat.* **1989**, *23*, 201–209.

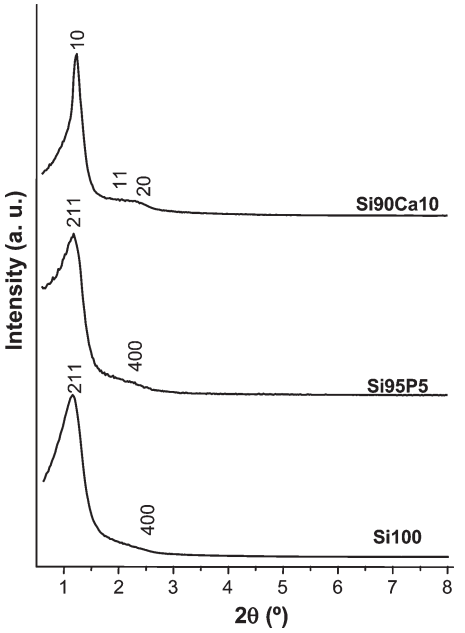

Figure 1. Low-angle powder X-ray diffraction (XRD) patterns obtained for calcined Si100, Si95P5, and Si90Ca10 compositions evaporated at 40 °C. Miller indexes for the corresponding cubic or hexagonal phases are indicated. Samples evaporated at 20 and 30 °C showed almost identical patterns.

Table 1. Mesoporous Structure (Space Groups) Observed for the Different Chemical Compositions and Solvent Evaporation Temperatures by XRD and TEM Studies

	Space Group		
sample	20 °C	30 °C	40 °C
Si100	$Ia\bar{3}d$	$Ia\bar{3}d$	$Ia\bar{3}d$
Si95P5	$Ia\bar{3}d$	$Ia\bar{3}d$	$Ia\bar{3}d$
Si90Ca10	*p6mm*	*p6mm*	*p6mm*
Si85Ca10P5	*p6mm*	*p6mm*/$Ia\bar{3}d$	$Ia\bar{3}d$

clearly dependent on the self-assembling temperature, evolving from a hydrophilic 2D-hexagonal phase *p6mm* toward a more hydrophobic $Ia\bar{3}d$ 3D-cubic bicontinuous structure, as the temperature increases. The XRD pattern for Si85Ca10P5 prepared at 20 °C clearly shows diffraction maxima at 1.18°, 2.02°, and 2.30°, which are assigned to reflections 10, 11, and 20, respectively, of a *p6mm* hexagonal phase. Si85Ca10P5 prepared at 30 °C exhibits a XRD pattern with maxima that cannot be assigned to a spatial group without a certain degree of ambiguity. In fact, the main peak at $2\theta = 1.14°$ exhibits a profile intermediate between the characteristic 10 reflection of a 2D-hexagonal phase and the 211 reflection of a 3D-cubic phase. In addition, the scattering observed between $2\theta = 1.8°$ and 2.4° cannot be clearly assigned to the 11 and 20 reflections of a *p6mm* planar group, or the 400 and 332 reflections of an $Ia\bar{3}d$ cubic phase. Further TEM studies were performed to provide a satisfactory answer. Finally, the XRD pattern for the calcined Si85Ca10P5 prepared at 40 °C shows diffraction maxima assignable to the 211, 400, and 332 reflections, respectively of a 3D-cubic $Ia\bar{3}d$ symmetry.

TEM studies confirm the results obtained by XRD. Figure 3 displays TEM images and the Fourier patterns

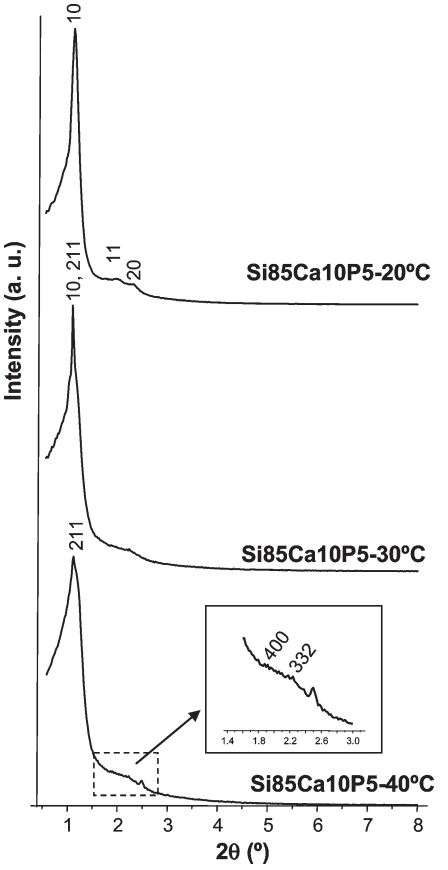

Figure 2. Low-angle powder X-ray diffraction (XRD) patterns obtained for calcined Si85Ca10P5 samples evaporated at 20, 30, and 40 °C. Miller indexes for the corresponding cubic or hexagonal phases are indicated.

obtained for Si100 (see Figure 3a) and Si95P5 (see Figure 3b) synthesized at 40 °C, showing typical images taken along the [111] direction of an $Ia\bar{3}d$ structure,[36] in agreement with XRD patterns. In contrast, the TEM image and the Fourier pattern for the Si90Ca10 sample (see Figure 3c) clearly evidence the formation of a 2D-hexagonal *p6mm* mesoporous structure. Identical results were observed for each composition, in the case of samples evaporated at 20 and 30 °C.

Figure 4 shows the TEM images for calcined Si85-Ca10P5 samples evaporated at 20, 30, and 40 °C during the self-assembly process. TEM images evidence the change of the mesoporous structure as a function of the self-assembly temperature. The Si85Ca10P5 sample obtained at 20 °C clearly evidences a 2D-hexagonal channel structure taken along the direction perpendicular to the channels, showing parallel planes with a *d*-spacing of 6.9 nm. When the evaporated temperature is 30 °C, the TEM images (see Figure 4b) show two certain domains. One domain (denoted as number 1 in Figure 4b) corresponds to the typical TEM image taken along the [111] direction of an $Ia\bar{3}d$ structure, showing values of $d_{211} = 7.9$ nm and $d_{220} = 6.9$ nm. In contrast, the second domain shows a typical 2D-hexagonal arrangement in the direction perpendicular to the channels with a value of $d_{10} = 6.9$ nm.

(36) Sakamoto, Y.; Kim, T. W.; Ryoo, R.; Terasaki, O. *Angew. Chem., Int. Ed.* **2004**, *43*, 5231–5234.

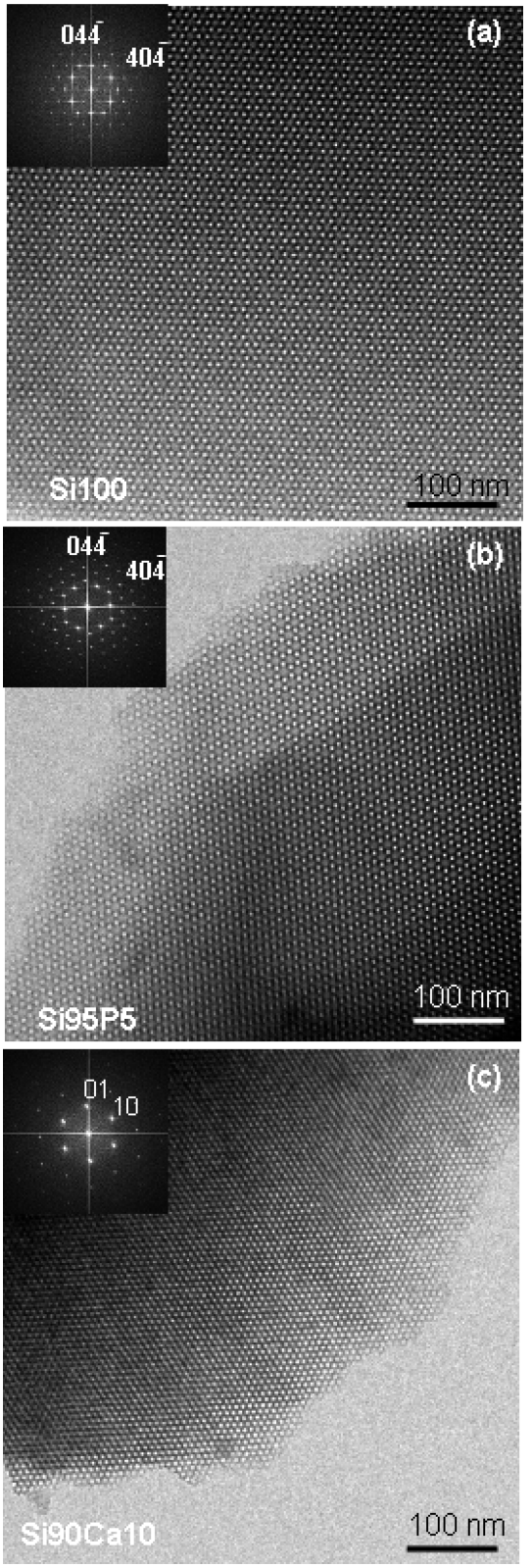

Figure 3. TEM images and Fourier patterns for calcined (a) Si100, (b) Si95P5, and (c) Si90Ca10 samples evaporated at 40 °C. Similar results were observed for each composition evaporated at 20 and 30 °C.

Therefore, TEM results demonstrate the phase transition occurred through the formation of a mixed ordering. In this transition, *p6mm* structure evolves toward a cubic $Ia\bar{3}d$ through the transformation of the 10 reflection of a 2D-hexagonal to the 220 reflection of the 3D-cubic structure.

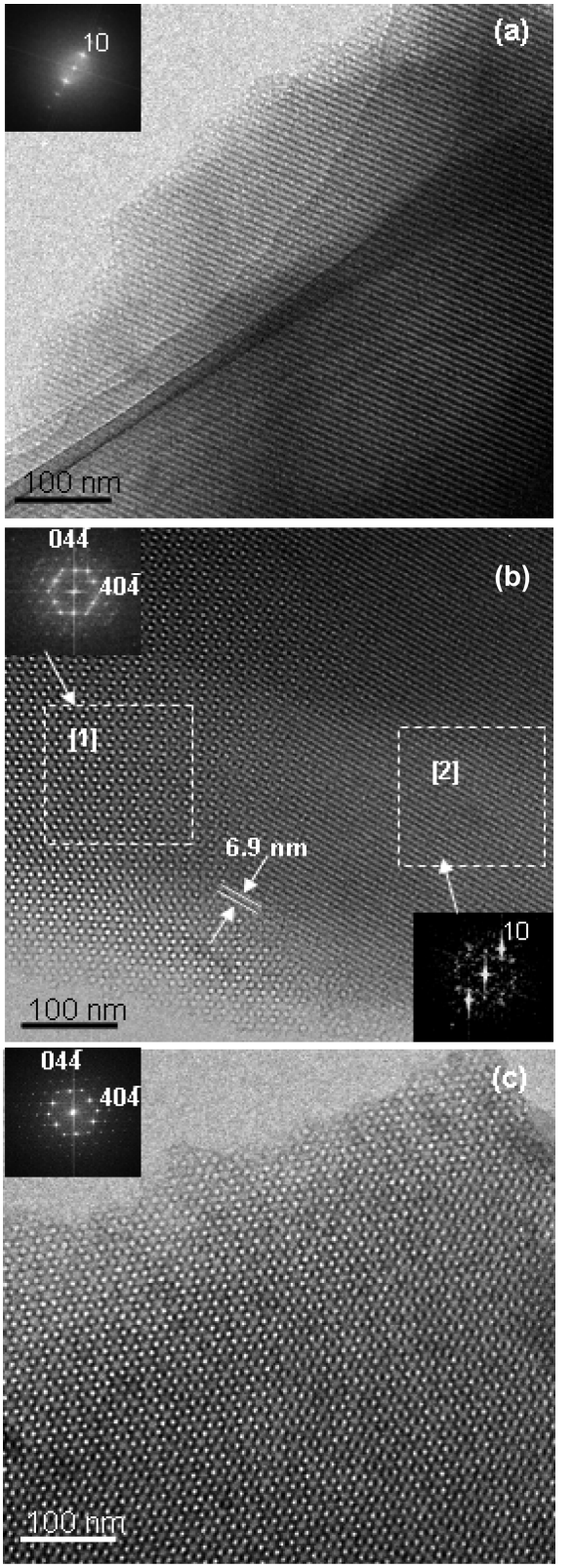

Figure 4. TEM images and Fourier patterns for calcined Si85Ca10P5 samples evaporated at (a) 20, (b) 30, and (c) 40 °C. Panel (a) shows a TEM image corresponding to a 2D-hexagonal structure. Panel (b) is a TEM image showing two well-defined domains (framed in dotted lines). FT patterns were obtained from these framed areas showing an $Ia\bar{3}d$ structure and a *p6mm* structure, respectively. Panel (c) shows TEM images that correspond to the [111] direction of a 3D-cubic structure.

This observation is consistent with the peak profiles observed by XRD for this sample, because the reflections

Table 2. Textural Properties of the Mesoporous Materials Prepared

sample	symmetry	space group	surface area, S_{BET} (m^2/g)[a]	total pore volume, V_p (cm^3/g)	pore diameter, D_P (nm)[b]	unit-cell parameter, a_0 (nm)[c]	wall thickness, t_{wall} (nm)
Si100	3D-cubic	$Ia\bar{3}d$	389.42	0.62	6.39	18.5	2.78
Si95P5	3D-cubic	$Ia\bar{3}d$	454.29	0.73	6.43	18.3	2.70
Si90Ca10	2D-hexagonal	*p6mm*	467.54	0.63	5.37	8.2	2.83
Si85Ca10P5−20 °C	2D-hexagonal	*p6mm*	472.74	0.63	5.37	8.6	3.23
Si85Ca10P5−40 °C	3D-cubic	$Ia\bar{3}d$	479.99	0.64	5.38	19.0	3.46

[a] Determined using the BET method. [b] Calculated using the BJH method. [c] Calculated by XRD.

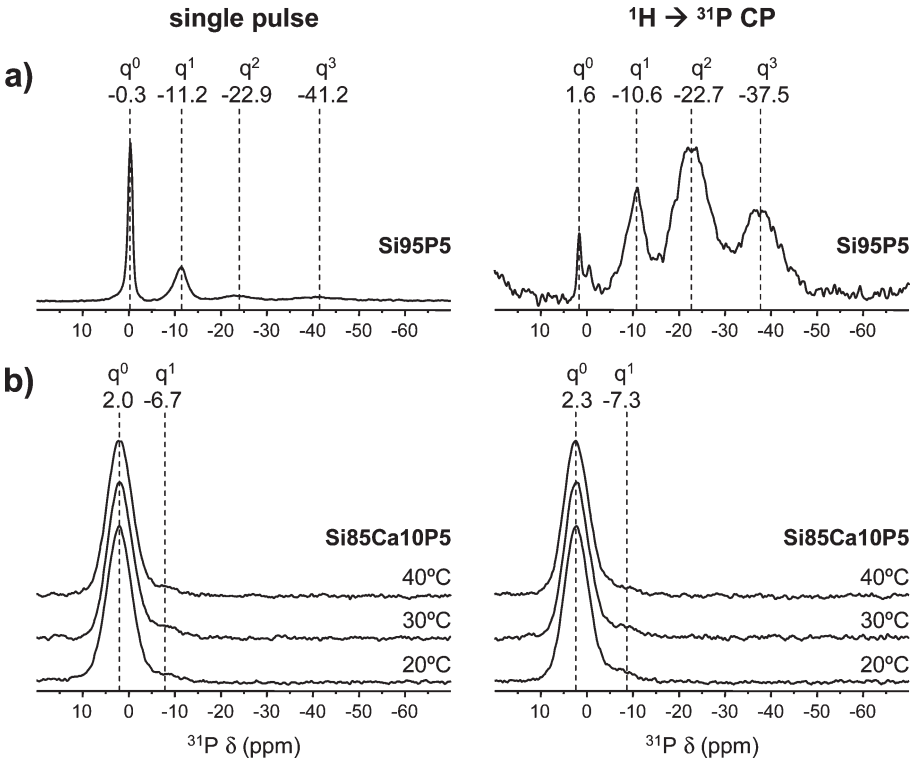

Figure 5. Solid-state ^{31}P single-pulse (left) and cross-polarization (right) MAS NMR spectra (with their respective q^n phosphorus environments shown at the top) of the (a) Si95P5 and (b) Si85Ca10P5 samples evaporated at 20, 30, and 40 °C.

observed must be a convolution of both coexisting phases. Finally, TEM observations of the Si85Ca10P5 sample at 40 °C evidence a cubic $Ia\bar{3}d$ mesoporous structure, as can be seen in Figure 4c, taken with an incidence beam parallel to the [111] direction, showing values of $d_{211} = 7.9$ and $d_{220} = 6.9$ nm.

Textural properties of the mesoporous glasses are collected in Table 2. All the isotherms showed curves characteristic of porous materials with type H1 hysteresis loops that correspond to cylindrical pores (see Figure S1 in the Supporting Information). The mesoporous glasses exhibit surface areas in the range of 390−480 m^2/g, similar to other MBGs previously reported.[1,31] Special attention should be given to the smaller pore diameters of the calcium-containing compositions (Si90Ca10 and Si85Ca10P5). These results are in clear agreement with an increase of the pore wall thickness, indicating a volume increase of the inorganic component during the mesophase formation. It must be highlighted that 2D-hexagonal Si85Ca10P5−20 °C and 3D-cubic Si85Ca10P5−40 °C show almost identical adsorption isotherms and pore size distributions, as well as S_{BET} and pore volume values (see Figure S2 in the Supporting Information).

^{31}P NMR. ^{31}P NMR spectroscopy was used to evaluate the local environment of P atoms, thus elucidating the phosphate species that is contained in the Si95P5 and Si85Ca10P5 (20, 30, and 40 °C) samples. Figure 5 shows the solid-stage ^{31}P MAS NMR spectra for both compositions. Spectra were recorded by single-pulse excitation (left) and by $^1H \rightarrow ^{31}P$ cross-polarization (right).

The spectrum that was recorded by single pulse for the Si95P5 sample shows four signals assignable to q^0, q^1, q^2, and q^3 phosphorus environments. In this case, q^0, q^1, q^2, and q^3 represent phosphorus atoms (denoted P*) present in the PO_4^{3-} species, $(NBO)_3P^*-(OP)$, $(NBO)_2-P^*-(OP_2)$, and $(NBO)-P^*(OP)_3$, respectively (NBO denotes a nonbonding oxygen, relative to another P atom). The presence of all these resonances in the Si95P5 spectrum indicates that an important amount of PO_4 tetrahedrons are forming ramified chains, thus acting as network formers, together with the SiO_2 network. However, the high percentage of q^0 also signifies that most of the P atoms are included as independent PO_4 tetrahedrons

Table 3. Chemical Shifts, Relative Peak Areas, and Silica Connectivity Obtained by Solid-State Single Pulse ^{29}Si MAS NMR

	Q^2		Q^3		Q^4		
	chemical shift	relative peak area	chemical shift	relative peak area	chemical shift	relative peak area	network connectivity
Si100			−101.0	14.6	−110.7	85.4	3.85
Si95P5	−94.1	4.7	−102.0	17.2	−110.6	78.1	3.73*
Si90Ca10	−91.8	3.6	−100.7	20.1	−109.9	76.3	3.72
Si85Ca10P5−20 °C	−93.1	2.2	−101.2	18.2	−110.4	79.6	3.77

* Network connectivity is underestimated for this sample, because only SiO_4 units (and not PO_4) have been considered as network formers in these calculations.

within the silica network. The $^1H\rightarrow^{31}P$ CP spectrum for the Si95P5 sample emphasizes resonances for q^2 and q^3, signifying that ramified polyphosphate chains are placed close to the protons (that is, at the material surface). Considering both spectra (SP and CP) for the Si95P5 sample, the results would agree with two main environments for the P_2O_5 into these materials. The first one would consist of individual PO_4 tetrahedrons (q^0) sited within the SiO_2 wall and bonded to four SiO_4 tetrahedrons in a regular environment (full width at half-maximum height (fwhm), equal to 1.2 ppm). The second one would consist of ramified polyphosphates, bonded to the end of silica chains and sited at the material surface. This situation can be explained in terms of the slower hydrolysis kinetic of the TEP, compared with TEOS.

Single-pulse excitation and $^1H\rightarrow^{31}P$ CP spectra for the Si85Ca10P5 samples show similar patterns. All the Si85Ca10P5 samples show a mean maximum of ∼2 ppm assigned at the q^0 environment. This signal shows a fwhm of *ca.* 6 ppm, which is typical of an amorphous orthophosphate. A second weak signal sited around −7 ppm appears for these samples. This resonance falls in the range of q^1 tetrahedra[37] and can be assigned to P−O−P or P−O−Si environments. Previous studies lead us to conclude that this signal is preferently attributed to a P−O−Si environment.[33] Both single-pulse and $^1H\rightarrow^{31}P$ CP spectra show very similar results. This fact indicates that, independent of the self-assembling temperature, the CaO presence in this system leads to the nucleation of an amorphous calcium phosphate (ACP), consuming all of the P_2O_5 and thus avoiding polyphosphate formation. To determine whether ACP clusters occur during the self-assembling of the Si85Ca10P5 sample or after surfactant calcinations, ^{31}P NMR spectra were recorded for this composition, evaporated at 20, 30, and 40 °C before calcination. The three spectra only showed one resonance that corresponded to the q^0 environment, thus indicating that calcium orthophosphate is formed before the subsequent thermal treatment (see Figure S3 in the Supporting Information), without the presence of other polyphosphate species.

^{29}Si NMR. ^{29}Si NMR spectroscopy was used to evaluate the network connectivity of MBGs as a function of chemical composition. Q^2, Q^3, and Q^4 represent the silicon atoms (denoted Si*) in $(NBO)_2Si^*-(OSi)_2$, $(NBO)Si^*-(OSi)_3$, and $Si^*(OSi)_4$ (NBO = nonbonding oxygen), respectively. (See Scheme S1 in the Supporting Information to facilitate an understanding of these resonances.) The signals in the region of −109 ppm to −111 ppm comes from Q^4; −100 ppm to −102 ppm comes from Q^3; and resonances at approximately −92 ppm comes from Q^2. Table 3 shows the chemical shifts, deconvoluted peak areas, and silica network connectivity for each composition.

One of the most determinant factors concerning mesoporous structure and bioactive behavior of MBGs, is the role of Ca^{2+} cations as network modifiers through the decreasing SiO_2 network density (see Table 3). Figure 6a shows the ^{29}Si NMR spectra recorded by single-pulse (left) and $^1H\rightarrow^{29}Si$ CP (right) analysis for the Si90Ca10 sample. SP ^{29}Si NMR spectrum shows two intense resonances, at −109.9 ppm and −100.7 ppm, corresponding to the Q^4 and $Q^3{}_H$ environments. In addition, there is a small shoulder at −91.8 ppm that could be assigned to $Q^3{}_{Ca}$, which is slightly more intense in the single-pulse spectrum (3.6 area %). More importantly, the proportion of Q^3 is lower in the environment close to protons (see the $^1H\rightarrow^{29}Si$ CP spectrum), indicating that Ca^{2+} cations responsible of Q^3 units are mostly sited within the silica walls (that is, well-distributed within the SiO_2 network of the Si90Ca10 sample).

The single-pulse ^{29}Si NMR spectrum for Si85Ca10P5−20 °C shows resonances corresponding to Q^4, Q^3, and $Q^2{}_H$ (see Table 3 and Figure 3b). No significant differences were observed in the spectra of the Si85Ca10P5 sample that was evaporated at 30 and 40 °C. The signal at −93.1 ppm is mainly assigned to the $Q^2{}_H$ (not to $Q^3{}_{Ca}$) environment attending to these criteria: (1) Ca^{2+} cations are mainly entrapped as ACP and (2) the $^1H\rightarrow^{29}Si$ CP spectrum shows this signal clearly emphasized. The small amount of free CaO (not entrapped as ACP) in this composition does not allow observing $Q^2{}_{Ca}$ environments when the spectrum is recorded by SP. However, $^1H\rightarrow^{29}Si$ CP spectrum shows a small signal at −85.4 ppm assigned to the $Q^2{}_{Ca}$ environment, highlighting the presence of this species close to the protons sited at the material surface. Contrary to the Si90Ca10 sample, the Si85Ca10P5 sample evidences a much more disrupted network at the surface (16.0% and 83.7% of Q^4 units for the Si85Ca10P5 and Si90Ca10 samples, respectively). This is clearly indicative of the joint presence of Ca^{2+} and $PO_4{}^{3-}$, resulting in calcium

(37) MacKenzie, K. J. D.; Smith, M. E. *Multinuclear Solid-State NMR of Inorganic Materials*; Pergamon Press: Amsterdam, 2002.

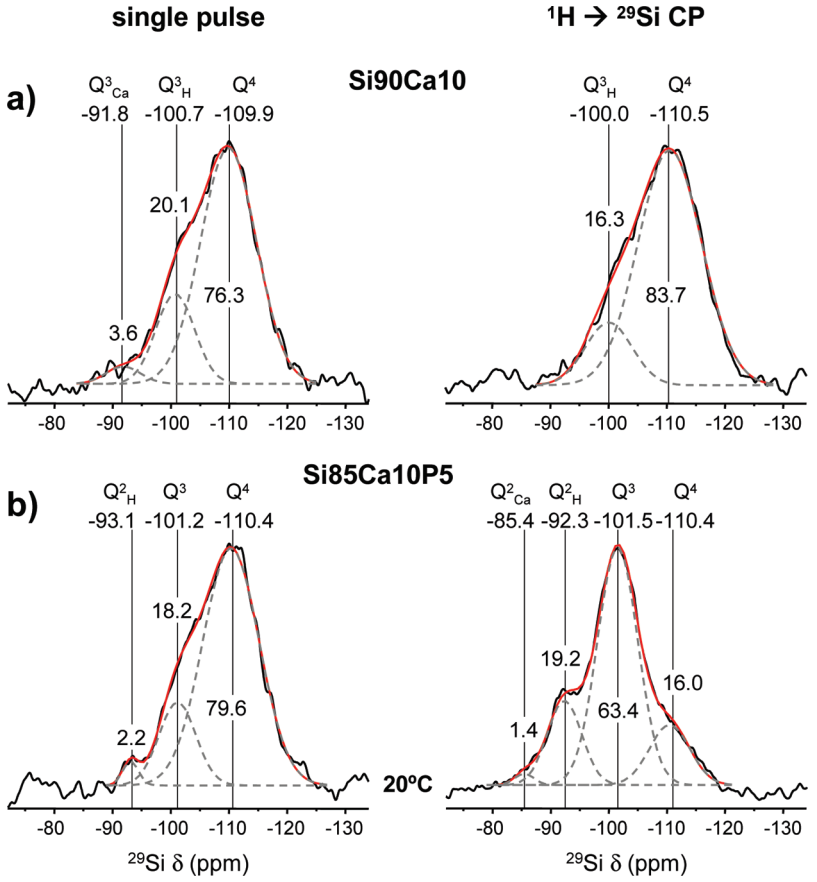

Figure 6. Solid-state ^{29}Si single-pulse (left) and cross-polarization (right) MAS NMR spectra of Si90Ca10 and Si85Ca10P5 (at 40 °C) samples. The areas for the Q^n units were calculated by Gaussian line-shape deconvolutions and are displayed by gray dotted lines (their relative populations are expressed as percentages).

phosphate clusters located at the wall surface, in agreement with the model previously reported for these types of materials.[33]

***In Vitro* Bioactivity Tests.** The surface reactivity of the mesoporous glasses was followed as a function of soaking time in SBF. *In vitro* bioactivity was assessed by analyzing the absorption band at the 560−600 cm^{-1} doublet in the FTIR spectra, corresponding to the phosphate formation in a crystalline environment. This method was proposed by Hench et al.,[35] and it is widely accepted for the assessment of bioactivity in SiO_2-based bioactive glasses. The Si100 and Si95P5 samples do not show bioactive behavior after one week in SBF (see Figure S4 in the Supporting Information). Figure 7 shows the FTIR spectra for the Si90Ca10 sample and the Si85Ca10P5 sample prepared at 20 and 40 °C (i.e., with *p6mm* hexagonal and $Ia\bar{3}d$ cubic structures). The Si90Ca10 sample (see Figure 7a) exhibits slow *in vitro* bioactive behavior under the conditions set for this study. After 24 h, a very weak absorption band is observed at 560 cm^{-1}, signifying the slight formation of amorphous calcium phosphate. After 7 days in SBF, a weak doublet at 560−600 cm^{-1} evidences the formation of a crystalline environment for the phosphate, which is indicative of the formation of an apatite-like phase. Si85Ca10P5−20 °C (Figure 7b) exhibits faster and more intense bioactive behavior. After 6 h, the singlet at 560 cm^{-1} is observed and only 8 h are needed for the observation of the PO_4^{3-} doublet, which is characteristic of the apatite formation. Figure 7c shows the *in vitro* bioactive behavior of the Si85Ca10P5−40 °C sample. As described previously, this sample is almost equivalent to the Si85Ca10P5−20 °C sample, with regard to the chemical composition and textural properties. In contrast, both samples show very different mesoporous structures. As can be observed from Figures 7b and 7c, the *in vitro* bioactive behaviors are almost identical. These results were confirmed with additional surface analyses with XRD, as a function of soaking time (see Figures S5 and S6 in the Supporting Information). In both cases, diffraction maxima can be assigned to the 211 and 002 reflections of an apatite phase that appear in the patterns without significant differences, in terms of peak intensity or profile.

Since the *in vitro* bioactive behavior results from the reaction between the material surface with the surrounding fluid, the ionic exchange between Ca^{2+} cations and H^+ from the SBF was determined. Figure 8 shows that a slight but significant $Ca^{2+}-H^+$ exchange can be observed for the Si85Ca10P5−40 °C sample, relative to the Si85Ca10P5−20 °C sample. These data signify that the pore ordering in bicontinuous cubic structures enhances the ionic exchange, relative to 2D hexagonal ones.

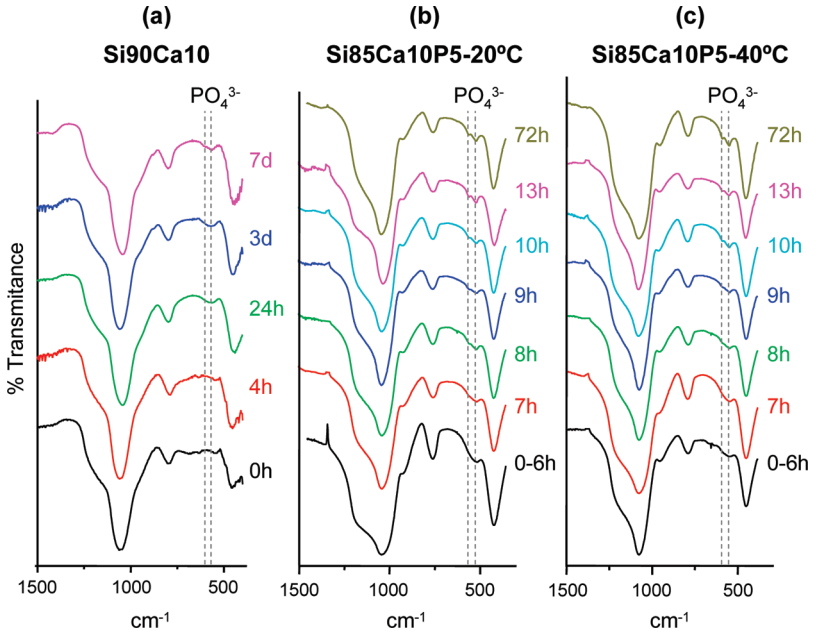

Figure 7. FTIR spectra obtained for the (a) Si90Ca10, (b) Si85Ca10P5−20 °C, and (c) Si85Ca10P5−40 °C samples soaked in SBF, as a function of time.

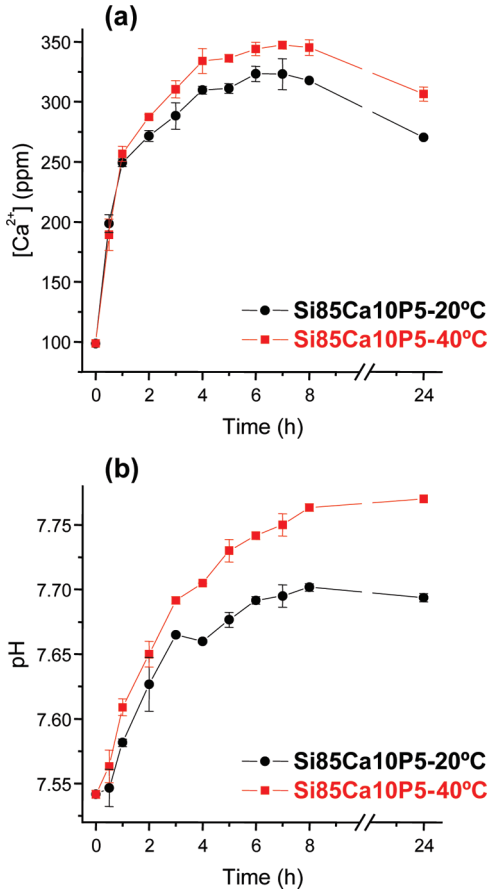

Figure 8. Variations of (a) Ca^{2+} content and (b) pH values of the SBF after soaking (−●−) the Si85Ca10P5−20 °C sample and (−■−) the Si85Ca10P5−40 °C sample.

Discussion

The results presented in this work demonstrate the fundamental role of amorphous calcium phosphate (ACP) on the mesoporous structure and bioactive behavior of SiO_2−CaO−P_2O_5 MBGs. In addition, the evaporation temperature during the EISA process seems to be an effective parameter to control the final mesostructure for a given ternary composition. Preparing ordered mesoporous glasses in a ternary system is not obvious. SiO_2−CaO−P_2O_5 contains both network formers (SiO_2 and P_2O_5) and a modifier (CaO) that disrupt the mesophase formation during the self-assembling of surfactant and inorganic species. For this reason, a more robust method, such as the EISA process, is required to prepare highly ordered materials in these systems. The EISA process occurs during the evaporation of the volatile solvent (in this case, ethanol) at low temperature (commonly "room temperature"). Our results demonstrate that strict control on the environmental conditions is required to prepare the desired MBGs.

In previous works, our research group has demonstrated that, by varying the CaO amount in SiO_2−CaO−P_2O_5, we can control the porous structure.[31] In this one, we demonstrate that, for the same composition (85SiO_2−10CaO−5P_2O_5, mol %), we can prepare MBGs with different mesoporous structures by changing the evaporation temperature within the 20−40 °C interval. The studies of the mesoporous structures of our materials demonstrates that, with the inorganic species/organic surfactant ratio used in this work, the systems exhibit a V_{inorg}/V_{org} ratio that was low enough to form hydrophobic structures with space groups such as $Ia\bar{3}d$. This is clear for highly dense inorganic phases exclusively prepared with network formers (SiO_2 and P_2O_5). The incorporation of 10% CaO (Si90Ca10), involves a lower connectivity index, as revealed by ^{29}Si NMR and, consequently, leads to inorganic phases with lower density. Because the V_{inorg}/V_{org} ratio increases in the Si90Ca10 composition, the mesophase arranges in a more hydrophilic structure that exhibits a 2D-hexagonal *p6mm* phase for any evaporation temperature.

On the other hand, the role of P_2O_5 is determinant in two aspects: mesoporous structure and bioactive behavior. In the case of the CaO-free composition (i.e., Si95P5), P_2O_5 is distributed as both PO_4 independent tetrahedrons within the silica network and polyphosphate chains at the silica surface. This second situation can be explained because of the slower hydrolysis of the P precursor (TEP), compared to the Si precursor (TEOS). Nevertheless, both situations involve a contribution to the network connectivity, resulting in hydrophobic 3D-cubic structures without bioactive behavior (i.e., the same situation as that for pure SiO_2 mesoporous material (Si100)). However, when P_2O_5 is part of the ternary system, its role changes completely. This is clear when comparing Si90Ca10 with Si85Ca10P5 MBGs. Si90Ca10 exhibits a 2D-hexagonal *p6mm* structure, as a consequence of the higher V_{inorg}/V_{org} ratio. Moreover, the combined studies of single-pulse and $^1H \rightarrow ^{29}Si$ CP NMR spectra indicate that Ca^{2+} cations are distributed within the inorganic silica walls but are not accumulated at the surface. In contrast, in the case of the Si85Ca10P5 sample, the presence of CaO and P_2O_5 leads to the formation of ACP clusters that are accumulated at the surface. In addition, the porous structure is not always 2D-hexagonal and is dependent on the evaporation temperature during the EISA process. Because Ca^{2+} is consumed to form ACP clusters, Ca^{2+} cations do not contribute to decrease SiO_2 connectivity and the hydrophobic 3D-cubic $Ia\bar{3}d$ phase can be formed, as a function of the evaporation temperature. It must be highlighted that 3D-cubic and 2D-hexagonal structures can coexist in the same material when an intermediate temperature (30 °C) is applied for evaporation. Certainly, ACP clusters also contribute to increase the inorganic volume. This is clear when calculating the wall thickness by N_2 adsorption porosimetry. However, the efficacy to create NBOs is lower than that provide by "free" Ca^{2+} cations. Consequently, hydrophobic phases can only occur at temperatures of < 30 °C.

The dependence of a mesoporous structure on the evaporation temperature can be explained in terms of a reduction of hydrogen interactions. In the case of nonionic triblock copolymers such as P123, the micelle size is strongly dependent on the hydrogen-bond interactions with the solvent, which becomes greater when hydrogen interactions are reduced. Consequently, the hydrophilic/hydrophobic ratio is reduced, favoring hydrophobic mesostructures such as cubic $Ia\bar{3}d$, as previously indicated by Zhao and co-workers for pure silica mesoporous materials obtained via the hydrothermal method.[38]

The main motivation for the synthesis and development of MBGs is their excellent bioactive behavior. In fact, the high textural properties of these compounds lead to long-term *in vitro* bioactivity, even for the calcium-free composition.[39] However, MBGs exhibit their maximum potential when CaO and P_2O_5 are both incorporated into the system. Recently, we have observed the fast kinetics of bonelike apatite formation onto these materials. For some compositions, < 1 h is sufficient for the nucleation of newly formed apatite under *in vitro* conditions.[32] To establish measurable differences between different compositions, we have set new conditions to increase the time for apatite crystallization. For this purpose, bioactivity tests were performed with MBG powders instead of compacted bodies, because the proximity of apatite nuclei enhances the apatite layer formation onto compact pieces. Under these conditions, important differences could be observed when comparing the binary system Si90Ca10 with the ternary composition Si85Ca10P5. The latest composition exhibits a much higher bioactive response, although the network former/modifier is identical. The difference is reflected in the local structure in both materials. The Si90Ca10 composition contains the Ca^{2+} cations distributed within the silica network, whereas the Si85Ca10P5 composition contains Ca^{2+} as calcium phosphate clusters at the wall surface. This involves two features: first, Ca^{2+} cations are more accessible to the surrounding fluids to initiate the bioactivity reaction cascade, and, second, the ACP clusters act as nucleation sites of the newly formed apatite.

By modifying the evaporation temperature of the Si85Ca10P5 composition, MBGs with the same composition and textural properties, but different porous structure, have been synthesized for the first time. In addition, MBGs with coexisting cubic and hexagonal phases have been isolated, as is the case of the Si85Ca10P5−30 °C sample. Recently, the influence of pore structure has been hypothesized as a factor that affects the bioactive behavior of MBGs. However, to date, different pore ordering in the SiO_2−CaO−P_2O_5 systems also has involved changes in molar composition and/or textural differences. Our bioactivity studies with 3D-cubic and 2D-hexagonal Si85Ca10P5 samples allow us to discriminate the pore array from other factors and show that differences in mesopore ordering are not determining the bioactive behavior of MBGs, when composition and texture are equivalent factors. Both *in vitro* bioactive processes exhibit equivalent behavior along the study, for 3D-cubic and 2D-hexagonal phases of the Si85Ca10P5 composition. The amount and accessibility of Ca^{2+} cations to the surrounding fluids, the presence of ACP clusters, the chemical composition, and the textural properties are the material-related factors that determine the *in vitro* bioactivity, independent of the mesopore ordering.

Conclusions

The mesoporous bioactive glass (MBG) $85SiO_2$−$10CaO$−$5P_2O_5$ (mol %) is formed by a silica network and amorphous calcium phosphate (ACP) clusters sited at the pore wall surface. In this system, the formation of hydrophilic 2D-hexagonal, hydrophobic 3D-cubic, or even mixed mesoporous structures is dependent on the solvent evaporation temperature.

The presence of CaO determines the *in vitro* bioactive behavior of multicomponent mesoporous glasses. Very

(38) Li, Z.; Chen, D. H.; Tu, B.; Zhao, D. Y. *Microporous Mesoporous Mater.* **2007**, *105*, 34–40.
(39) Izquierdo-Barba, I.; Ruiz-González, L.; Doadrio, J. C.; González-Calbet, J. M.; Vallet-Regí, M. *Solid State Sci.* **2005**, *7*, 983–989.

important kinetic differences are observed when Ca^{2+} cations are dispersed into the SiO_2 network or are forming segregated calcium orthophosphate clusters at the surface.

2D-hexagonal Si85Ca10P5 and 3D-cubic Si85Ca10P5 samples exhibit almost identical *in vitro* bioactive behavior, although a slight but significant $Ca^{2+}-H^{+}$ exchange can be observed for the bicontinuous cubic sample, with respect to the hexagonal one. This observation indicates that chemical composition, textural properties, and the presence of accessible ACP clusters determine the *in vitro* bioactive behavior, independent of the mesopore structure.

Acknowledgment. This work was supported by the Spanish CICYT (through Project No. MAT2008-00736) and by the Comunidad Autónoma de Madrid (through Project No. S-0505/MAT/0324). We also thank to the CAI Electron Microscopy Center, CAI Nuclear Magnetic Resonance and Fernando Conde (CAI X-ray Diffraction), Universidad Complutense de Madrid, for their valuable technical assistance.

Supporting Information Available: Nominal compositions and reactants used to prepare mesoporous materials in MBGs (Table S1). Isotherms of mesoporous materials in this work (Figures S1 and S2). NMR studies of the Si85Ca10P5 composition before calcination (Figure S3). Negative bioactivity tests for Si100 and Si95P5 samples (Figure S4). Powder XRD patterns of Si85Ca10P5 evaporated at 20 and 40 °C after soaking in simulated body fluid (SBF) (Figures S5 and S6). Schematic depiction of Q^n_H and Q^n_{Ca} assignments in solid-state ^{29}Si NMR (Scheme 1). (PDF) This material is available free of charge via the Internet at http://pubs.acs.org.